Circulating Current Suppressing Strategy for MMC-HVDC Based on Nonideal Proportional Resonant Controllers Under Unbalanced Grid Conditions

Shaohua Li, Xiuli Wang, *Member, IEEE*, Zhiqing Yao, Tai Li, and Zhong Peng

***Abstract*—Modular multilevel converter (MMC) is considered as a promising topology for voltage-source converter (VSC) high-voltage, direct current (HVDC) applications. This paper presents a new control strategy for MMC-HVDC under unbalanced grid conditions. First, a new inner loop current control strategy based on nonideal proportional resonant (PR) controllers in stationary $\alpha\beta$ frame is designed, which is more concise compared to the existing dual sequence current control scheme. Second, an analytical expression for circulating current is obtained which shows that the circulating currents will be asymmetric under unbalanced grid conditions and can be decomposed into positive-, negative-, and zero-sequence component. In order to suppress all these components, a new circulating current suppressing strategy is analyzed and designed also based on nonideal PR controllers. Application of nonideal PR controllers makes the control system well adapt to the fluctuation of grid frequency. The effectiveness of the proposed control strategy is verified through a simulation case of a 251-level MMC-HVDC transmission system using real-time digital simulator.**

***Index Terms*—Circulating current, high voltage direct current (HVDC) transmission, modular multilevel converter (MMC), nonideal proportional resonant (PR), real-time digital simulator (RTDS).**

I. Introduction

HIGH-VOLTAGE, direct current transmission based on modular multilevel converters (MMC-HVDC) is a new voltage-source converter (VSC) technology. Compared to traditional two-level or three-level converter, MMC offers several advantages including a reduction in switching losses, upgraded capacity, fewer electromagnetic compatibility issues, better fault management, and so on [1]–[3]. MMC is currently one of the most promising topologies in the HVDC field [4].

The control system plays an important role in the performance of MMC-HVDC. There are two common types of control system in MMC-HVDC. One is based on *dq* synchronous rotating frame (SRF), and the other is based on stationary frame. Vector current control in *dq* SRF performs well under balanced grid conditions, however, a dual current control scheme including positive- and negative-sequence vector current controller should be adopted under unbalanced grid conditions [5]. Its performance is investigated in [6], [7]. Despite performing well in unbalanced conditions, the dual current control scheme has some disadvantages, one being its relatively complicated structure. Recently, a proportional resonant (PR) control strategy based on stationary frame has become popular in grid connected converters [8]. This control strategy can track a sinusoidal reference at a certain frequency with zero steady-state error. Under unbalanced grid conditions, using PR controllers based on stationary frame in MMC-HVDC control system can simplify the control structure, because decomposing the positive-, and negative-sequence *dq* components of current and voltage can be avoided [9]–[11]. However, since the PR controller introduces an infinite gain at its resonant frequency, any small frequency deviation of the reference signal may lead to a large tracking error.

Circulating current is a potential problem coming with MMC [12]–[15]. It increases current stress and introduces additional conduction loss to the system. Under balanced grid conditions, the negative-sequence component of circulating current in each arm flows at twice the nominal frequency. Under unbalanced grid conditions, circulating current will have positive- and zero-sequence components in addition to the negative-sequence component [16]. The elimination/minimization of circulating current in converter arms is one of the main technical challenges of MMC [17]. One way to decrease the amplitude of the circulating current is to increase inductance in each arm. But this technique cannot completely eliminate the circulating current and is not cost-effective since the high-voltage inductors are very expensive [15], [17]. Another approach is to apply circulating current suppressing control strategy. Recently, some control strategies have been introduced, but they have some shortages. Tu *et al*. [18] proposed a supplementary dc voltage ripple suppressing controller to eliminate the zero-sequence component in the circulating current. This method, however, required the measurement of the valve section voltage of each arm, and it

Manuscript received September 24, 2013; revised April 12, 2014; accepted November 23, 2013. Date of publication June 5, 2014; date of current version August 26, 2014. Recommended for publication by Associate Editor M. T. Bina.

S. Li is with the Department of Electrical Engineering, Xi'an Jiaotong University, Xi'an 710049, China, and also with the XJ Electric Co., Ltd., Xuchang 461000, China (e-mail: 380403132@qq.com).

X. Wang is with the Department of Electrical Engineering, Xi'an Jiaotong University, Xi'an 710049, China (e-mail: xiuliw@mail.xjtu.edu.cn).

Z. Yao is with the Department of Electrical Engineering, Huazhong University of Science and Technology, Wuhan 430074, China, and also with the KETOP Electrical Research Institute, Xuchang 461000, China (e-mail: zhiqingy@dlwg.net).

T. Li and Z. Peng are with the XJ Electric Co., Ltd., Xuchang 461000, China (e-mail: taidouli@163.com; 554007683@qq.com).

Color versions of one or more of the figures in this paper are available online at http://ieeexplore.ieee.org.

Digital Object Identifier 10.1109/TPEL.2014.2329059

0885-8993 © 2014 IEEE. Personal use is permitted, but republication/redistribution requires IEEE permission.
See http://www.ieee.org/publications_standards/publications/rights/index.html for more information.

could not eliminate the positive-sequence component. Furthermore, its control structure was complicated. Yuebin *et al.* [11] proposed a control method for circulating current suppressing in the $\alpha\beta_0$ stationary frame, which used high-pass filters to extract the double-line frequency component from circulating current. This filters influenced the dynamic performance of the controller, and the response of the ideal PR controller would deteriorate when system frequency varied. Moon *et al.* [16] proposed a new circulating current suppressing strategy. Four proportional integral resonant (PIR) controllers were used in this method. Three of them were employed to eliminate the positive- and negative-sequence components in circulating current, and the last one was for eliminating the zero-sequence component. The input of the PIR controller for eliminating zero-sequence component was the difference between dc current and its reference, which was derived from the steady dc power divided by constant dc voltage. Obviously, this was a very strict requirement, and the simulation case was based on a single terminal system (the other was a constant dc voltage source).

Voltage balancing among the SM capacitors is another key part to the performance of MMC. Some voltage-balancing algorithms, by sorting the capacitors' voltage, were proposed in [12], [19]–[21]. The SMs with the lowest or highest capacitor voltages were triggered according to the direction of the arm current.

This paper addresses two main issues of MMC (i.e., the inner loop current control and the circulating current suppression). A new inner loop current control method using nonideal PR controllers in $\alpha\beta$ stationary frame, and a new circulating current suppressing strategy which is also based on nonideal PR controllers in *abc* stationary frame are proposed. Compared to other published control strategies, the new strategy has the following advantages: reduced number of required controllers, improved ability to adapt to frequency fluctuation, reduced calculation load due to succinct arithmetic, and effective control both MMC-HVDC terminals under unbalanced grid conditions. The performance is introduced in detail in Section IV.

The remainder of this paper is organized as follows. In Section II, the mathematical model and fundamental control principle of MMC are presented. Section III describes the inner loop current control and circulating current suppressing strategy, which are both based on nonideal PR controllers. Simulation results are provided in Section IV, where nonreal time mode simulation on RTDS is performed to test the performance of the proposed method. Conclusion is drawn in Section V. Finally, the appendix details the parameters design for the inner loop current nonideal PR controllers.

II. Basic Structure and Mathematic Model of MMC

A. Basic Structure

The basic circuit structure of a three-phase MMC is shown in Fig. 1(a). It consists of six arms. Each arm includes a total of *N* submodules (SM) and one series inductor L_0. Two arms in the same phase comprise a phase unit. A single SM is shown in Fig. 1(b). The SM output voltage only has two values:

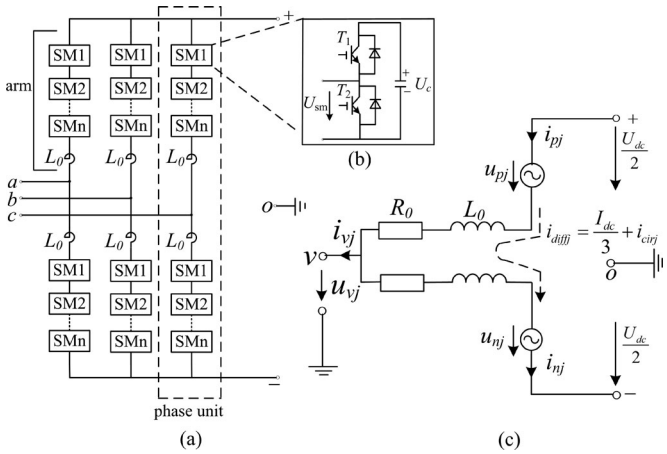

Fig. 1. Basic structure of MMC: (a) Circuit diagram of the MMC. (b) Structure of SM. (c) Single-line equivalent circuit of the three-phase MMC.

1) $U_{sm} = U_c$ when the upper insulated gate bipolar transistor (IGBT) is ON and the lower one is OFF;
2) $U_{sm} = 0$ when the upper IGBT is OFF and the lower one is ON.

B. Mathematical Model

The single-line equivalent circuit of the three-phase MMC is shown in Fig. 1(c). L_0 is the arm inductor, R_0 denotes the arm losses, $U_{\rm dc}$ is the total dc bus voltage. u_{vj} $(j = a, b, c)$ is the converter output voltage of phase *j* at point V, i_{vj} $(j = a, b, c)$ is the line current. The valve section (excluding L_0) voltage of six arms are expressed as u_{pj} and u_{nj} $(j = a, b, c$, and the subscript *p* denotes the upper arm, while *n* denotes the lower arm); i_{pj} and i_{nj} are the upper and lower arm currents, respectively.

The characteristics of MMC can be expressed as follows [13]:

$$u_{vj} = e_j - \frac{R_0}{2} i_{vj} - \frac{L_0}{2} \frac{di_{vj}}{dt} \ (j = a, b, c) \tag{1}$$

$$\begin{aligned} u_{diffj} &= L_0 \frac{di_{diffj}}{dt} + R_0 i_{diffj} \\ &= \frac{1}{2} \left[U_{\rm dc} - (u_{pj} + u_{nj}) \right] (j = a, b, c) \end{aligned} \tag{2}$$

where e_j in (1) is the inner imaginary voltage generated in phase *j* and can be expressed as

$$e_j = \frac{u_{nj} - u_{pj}}{2}. \tag{3}$$

u_{diffj} in (2) is the MMC inner unbalanced voltage, i_{diffj} in (2) is the inner unbalanced current of phase *j* and is given as

$$i_{diffj} = \frac{i_{pj} + i_{nj}}{2} = \frac{I_{\rm dc}}{3} + i_{cirj} \tag{4}$$

where $I_{\rm dc}/3$ is the inner unbalanced current's dc component and i_{cirj} is the inner unbalanced current's ac component, which is the circulating current component.

Based on (1) and (2), the line current i_{vj} can be controlled by e_j, while the inner circulating current i_{diffj} can be controlled by u_{diffj}. According to (2) and (3), the reference of arm voltage

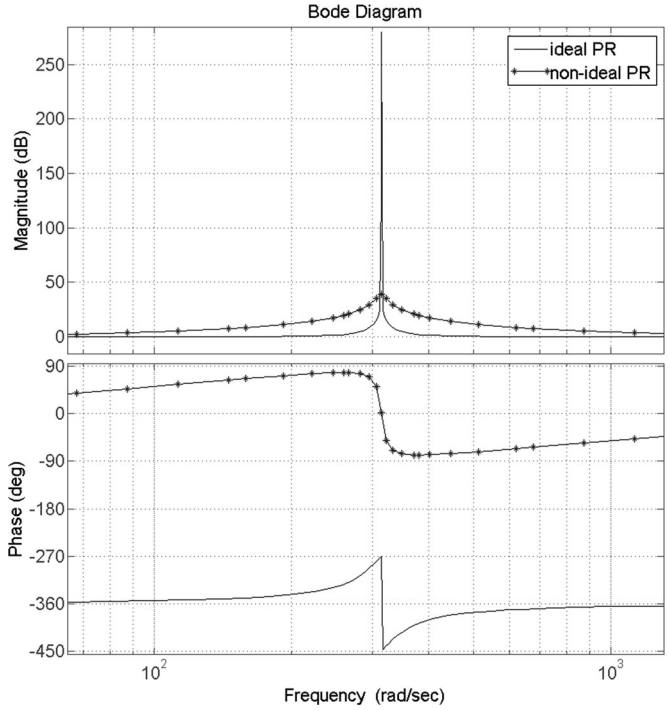

Fig. 2. Bode diagram of ideal PR and nonideal PR controller.

can be defined as

$$u_{pj\_\mathrm{ref}} = \frac{U_{\mathrm{dc}}}{2} - e_{j\_\mathrm{ref}} - u_{diffj\_\mathrm{ref}} \tag{5a}$$

$$u_{nj\_\mathrm{ref}} = \frac{U_{\mathrm{dc}}}{2} + e_{j\_\mathrm{ref}} - u_{diffj\_\mathrm{ref}}. \tag{5b}$$

In (5), the inner imaginary voltage reference e_{j_ref} is obtained from the inner loop current controllers [14], while the inner unbalanced voltage reference u_{diffj_ref} is obtained from the circulating current suppressing controller, which can be used to reduce the three-phase inner circulating currents in MMC. It can be inferred from (1)–(5) that the line current i_{vj} and inner unbalanced current i_{diffj} can be controlled respectively, and the total objective can be obtained by adding outputs of the two controllers.

III. Design of the Control System Under Unbalanced Grid Conditions

A. Concept of Nonideal PR Controller

Transfer functions of ideal and nonideal PR controller are respectively given by [22]

$$G(s) = k_p + \frac{k_r s}{s^2 + \omega_0^2} \tag{6a}$$

$$G(s) = k_p + \frac{2k_r\omega_c s}{s^2 + 2\omega_c s + \omega_0^2} \tag{6b}$$

where k_p, k_r, ω_0, and ω_c represent proportional gain, resonant gain, resonant frequency, and cutoff frequency, respectively.

It can be inferred from Fig. 2 that compared to ideal PR controller, nonideal PR controller increases the error of tracking the reference signal at resonant frequency, but it reduces the sensitivity to the frequency deviation. As a result, the selection of ω_c is a compromise between the reduction of sensitivity and the error in tracking the reference signal [22]. The parameter k_p basically determines the dynamic performance of the system. And the parameter k_r basically determines the steady gain and phase shift of the system at resonant frequency.

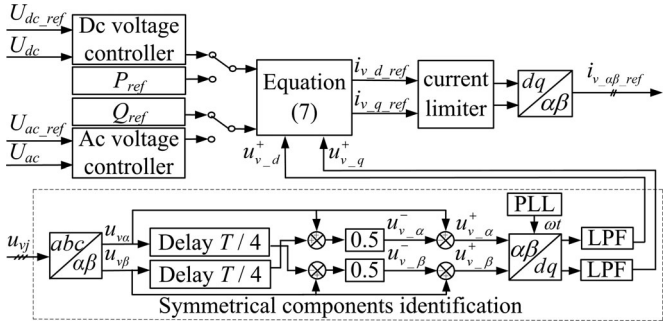

Fig. 3. Block diagram of the outer loop power controller.

B. Outer Loop Power Control

The outer loop power control is designed to provide the command references for the inner loop current control. There are two different power controllers for conventional converters under unbalanced conditions. One is developed to eliminate negative-sequence current components to keep ac currents balanced; the other is developed to eliminate the double line-frequency ripples in the dc-side voltage by suppressing the double line-frequency ripples in the three-phase active power input to the converter [23]. However, the objective of the outer loop power controller to eliminate double line-frequency ripples in dc-side voltage is not achieved in MMC [24]. Thus, this paper adopts the first scheme. The reference of line current in *dq* SRF is equal to the positive-sequence current reference when the negative-sequence current reference is zero. According to instantaneous reactive power theory, it can be expressed by

$$I_{v\_d\_\mathrm{ref}} = I^{+}_{v\_d\_\mathrm{ref}} = \frac{P_{\mathrm{ref}} \cdot u^{+}_{v\_d} - Q_{\mathrm{ref}} \cdot u^{+}_{v\_q}}{(u^{+}_{v\_d})^2 + (u^{+}_{v\_q})^2} \tag{7a}$$

$$I_{v\_q\_\mathrm{ref}} = I^{+}_{v\_q\_\mathrm{ref}} = \frac{P_{\mathrm{ref}} \cdot u^{+}_{v\_q} + Q_{\mathrm{ref}} \cdot u^{+}_{v\_d}}{(u^{+}_{v\_d})^2 + (u^{+}_{v\_q})^2} \tag{7b}$$

where P_{ref} is active power reference, Q_{ref} is reactive power reference, $u^{+}_{v\_d}$ and $u^{+}_{v\_q}$ are the positive-sequence components of u_v in *dq* SRF. P_{ref} is set to a constant value or derived from dc voltage controller, while Q_{ref} is set to a constant value or derived from ac voltage controller.

Since the inner current controller is based on $\alpha\beta$ static frame, $i_{v\_d\_\mathrm{ref}}$ and $i_{v\_q\_\mathrm{ref}}$ based on *dq* rotating frame should be transformed to $i_{v\_\alpha\_\mathrm{ref}}$ and $i_{v\_\beta\_\mathrm{ref}}$. The outer loop power control block diagram is shown as Fig. 3.

In Fig. 3, the dc voltage controller generates the active power reference for (7), while the ac voltage controller generates the reactive power reference. For a two terminal MMC-HVDC

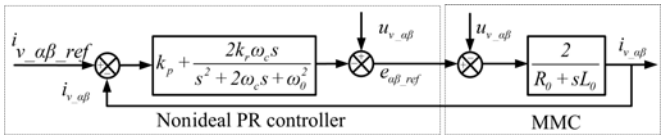

Fig. 4. Diagram of the inner loop current controller.

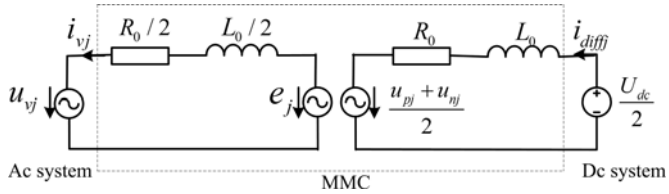

Fig. 5. AC/DC decomposed model of single phase MMC.

transmission system, one terminal controls the dc voltage, while the other terminal controls the active power. Both terminals can choose to control its ac voltage or reactive power. The *T* in Fig. 3 is equal to $2\pi/\omega_0$. A low-pass filter (LPF) is used to eliminate the interference of high order harmonics from measured signals. The phase signal ωt is generated by phase locked loop (PLL). A current limiter block is used to prevent the over current of i_{vj}.

C. Inner Loop Current Control

Equation (1) can be rewritten in stationary $\alpha\beta$ frame by Clark's transformation, shown as

$$u_{v\_\alpha\beta} = e_{\alpha\beta} - \frac{R_0}{2} i_{v\_\alpha\beta} - \frac{L_0}{2}\frac{di_{v\_\alpha\beta}}{dt}. \tag{8}$$

According to Laplace transformation, (8) can be written as

$$e_{\alpha\beta}(s) - u_{v\_\alpha\beta}(s) = \frac{R_0 + sL_0}{2} i_{v\_\alpha\beta}(s) \tag{9}$$

where $u_{v\_\alpha\beta}(s) = [u_{v\_\alpha}(s), u_{v\_\beta}(s)]^T$, $e_{\alpha\beta}(s) = [e_\alpha(s), e_\beta(s)]^T$, $i_{v\_\alpha\beta}(s) = [i_{v\_\alpha}(s), i_{v\_\beta}(s)]^T$. According to (5) and (9), $i_{v\_\alpha\beta}(s)$ can be controlled to the target value through controlling the $e_{\alpha\beta}(s)$. Since $i_{v\_\alpha\beta}(s)$ are sinusoidal signals, nonideal PR controllers are employed. Block diagram of the inner loop current control is shown as Fig. 4. The negative-sequence component in ac current is eliminated under unbalanced grid conditions because $i_{v\_\alpha\beta\_ref}$ only contains positive-sequence component.

The control strategy shown in Fig. 4 has the following advantages:

1) compared to control strategy in stationary *abc* reference frame, this control strategy in $\alpha\beta$ reference frame reduces one controller;
2) compared to control strategy in *dq* SRF, this control strategy reduces a negative-sequence current controller, which is more stable because of no PLL, and faster because of less calculated load;
3) compared to ideal PR controller, the control strategy is more effective when the frequency of grid varies.

Parameters design of the nonideal PR controller is shown in appendix.

D. Circulating Current Suppressing Control

From (1) and (2), equivalent circuit of the single-phase MMC can be deduced as Fig. 5 [18].

In Fig. 5, u_{vj} and i_{vj} are phase voltage and line current of the ac output of phase j in MMC. Under unbalanced grid conditions, there will be no zero-sequence voltage and zero-sequence current at the valve side of the converter transformer because the converter transformer is always Y/Δ connection. So the voltage and current of the phase *a* can be expressed by

$$u_{va} = U_m^+ \cos(\omega t + \theta^+) + U_m^- \cos(\omega t + \theta^-) \tag{10}$$

$$i_{va} = I_m^+ \cos(\omega t + \varphi^+) + I_m^- \cos(\omega t + \varphi^-) \tag{11}$$

$$i_{va} = i_{pa} - i_{na} \tag{12}$$

where U_m^+, U_m^- are the positive- and negative-sequence voltage amplitude of the ac grid, respectively, and correspondingly θ^+, θ^- are the initial phase. I_m^+, I_m^- are the positive- and negative-sequence current amplitude of the ac grid, respectively, and correspondingly φ^+, φ^- are the initial phase.

If ignoring the inner loss of converter and the influence of inductors, the instantaneous power of the ac port should be equal to the dc port

$$u_{va} i_{va} = \frac{U_{\rm dc}}{2} i_{diffa}. \tag{13}$$

Substituting (4), (10)–(12) into (13), we can obtain

It can be inferred from (14a) and (14b) shown as the bottom of the next page, that under balanced grid conditions, the upper and lower arm currents are both composed of dc component, fundamental frequency component, and negative-sequence component at double line-frequency in three phases of MMC. Under unbalanced grid conditions, the upper and lower arm currents contain dc component, positive- and negative-sequence component at fundamental frequency, positive-, negative- and zero-sequence component at double line-frequency.

Equation (14c) shown as the bottom of the next page, describes the components of inner unbalanced current. i_{pa0} indicates that dc current will not be average in three-phase arms under unbalanced grid conditions. i_{pa2}^+ and i_{pa2}^- indicate that, under unbalanced grid conditions, there will be positive- and negative-sequence current at double line-frequency in three-phase arms, which cannot flow into dc line, but increase loss of MMC. i_{pa2}^0 indicates that under unbalanced grid conditions, there will be zero-sequence current at double line-frequency, which can flow into dc line and generate second harmonic in dc current. Equation (14d) shown as the bottom of the next page, describes that the circulating current is composed of i_{pa2}^+, i_{pa2}^-, and i_{pa2}^0. Equation (14e) shown as the bottom of the next page, indicates that the zero-sequence currents of three phases at double line-frequency flow into dc line under unbalanced grid conditions.

A new circulating current suppressing controller in *abc* frame is proposed to eliminate the double line-frequency components in the inner unbalanced current. Similar to the control strategy

of the inner current loop, nonideal PR controller is employed. The difference is that the resonant frequency should be $2\omega_0$. Correspondingly, the cutoff frequency ω_c should be two times of the one in the inner loop current controller. The reference of i_{diffj} is set to one-third of the dc current measured. A LPF is used to extract the dc component from the dc current measured, which contains double line-frequency component under unbalanced grid conditions. The block diagram of circulating current suppressing controller is shown as Fig. 6.

The new control strategy has following advantages:

1) effectively suppressing positive-, negative-, and zero-sequence circulating currents at double-line frequency;

$$i_{pa}=\underbrace{\frac{U_m^+I_m^+}{U_{\rm dc}}\cos(\theta^+-\varphi^+)+\frac{U_m^-I_m^-}{U_{\rm dc}}\cos(\theta^--\varphi^-)+\frac{U_m^+I_m^-}{U_{\rm dc}}\cos(\theta^+-\varphi^-)+\frac{U_m^-I_m^+}{U_{\rm dc}}\cos(\theta^--\varphi^+)}_{i_{pa0}\,(\text{dc component})}$$
$$+\underbrace{\frac{I_m^+}{2}\cos(\omega t+\varphi^+)+\frac{I_m^-}{2}\cos(\omega t+\varphi^-)}_{i_{pa1}\,(\text{fundamental frequency component})}+\underbrace{\frac{U_m^-I_m^-}{U_{\rm dc}}\cos(2\omega t+\theta^-+\varphi^-)}_{i^+_{pa2}\,(\text{positive-sequence component at double line-frequency})}$$
$$+\underbrace{\frac{U_m^+I_m^+}{U_{\rm dc}}\cos(2\omega t+\theta^++\varphi^+)}_{i^-_{pa2}\,(\text{negative-sequence component at double line-frequency})}+\underbrace{\frac{U_m^+I_m^-}{U_{\rm dc}}\cos(2\omega t+\theta^++\varphi^-)+\frac{U_m^-I_m^+}{U_{\rm dc}}\cos(2\omega t+\theta^-+\varphi^+)}_{i^0_{pa2}\,(\text{zero-sequence component at double line-frequency})} \tag{14a}$$

$$i_{na}=\underbrace{\frac{U_m^+I_m^+}{U_{\rm dc}}\cos(\theta^+-\varphi^+)+\frac{U_m^-I_m^-}{U_{\rm dc}}\cos(\theta^--\varphi^-)+\frac{U_m^+I_m^-}{U_{\rm dc}}\cos(\theta^+-\varphi^-)+\frac{U_m^-I_m^+}{U_{\rm dc}}\cos(\theta^--\varphi^+)}_{i_{pa0}\,(\text{dc component})}$$
$$-\underbrace{\frac{I_m^+}{2}\cos(\omega t+\varphi^+)-\frac{I_m^-}{2}\cos(\omega t+\varphi^-)}_{i_{pa1}\,(\text{fundamental frequency component})}+\underbrace{\frac{U_m^-I_m^-}{U_{\rm dc}}\cos(2\omega t+\theta^-+\varphi^-)}_{i^+_{pa2}\,(\text{positive-sequence component at double line-frequency})}$$
$$+\underbrace{\frac{U_m^+I_m^+}{U_{\rm dc}}\cos(2\omega t+\theta^++\varphi^+)}_{i^-_{pa2}\,(\text{negative-sequence component at double line-frequency})}+\underbrace{\frac{U_m^+I_m^-}{U_{\rm dc}}\cos(2\omega t+\theta^++\varphi^-)+\frac{U_m^-I_m^+}{U_{\rm dc}}\cos(2\omega t+\theta^-+\varphi^+)}_{i^0_{pa2}\,(\text{zero-sequence component at double line-frequency})} \tag{14b}$$

$$i_{diffa}=\underbrace{\frac{U_m^+I_m^+}{U_{\rm dc}}\cos(\theta^+-\varphi^+)+\frac{U_m^-I_m^-}{U_{\rm dc}}\cos(\theta^--\varphi^-)+\frac{U_m^+I_m^-}{U_{\rm dc}}\cos(\theta^+-\varphi^-)+\frac{U_m^-I_m^+}{U_{\rm dc}}\cos(\theta^--\varphi^+)}_{i_{pa0}\,(\text{dc component})}$$
$$+\underbrace{\frac{U_m^-I_m^-}{U_{\rm dc}}\cos(2\omega t+\theta^-+\varphi^-)}_{i^+_{pa2}\,(\text{positive-sequence component at double line-frequency})}+\underbrace{\frac{U_m^+I_m^+}{U_{\rm dc}}\cos(2\omega t+\theta^++\varphi^+)}_{i^-_{pa2}\,(\text{negative-sequence component at double line-frequency})}$$
$$+\underbrace{\frac{U_m^+I_m^-}{U_{\rm dc}}\cos(2\omega t+\theta^++\varphi^-)+\frac{U_m^-I_m^+}{U_{\rm dc}}\cos(2\omega t+\theta^-+\varphi^+)}_{i^0_{pa2}\,(\text{zero-sequence component at double line-frequency})} \tag{14c}$$

$$i_{cira}=\underbrace{\frac{U_m^-I_m^-}{U_{\rm dc}}\cos(2\omega t+\theta^-+\varphi^-)}_{i^+_{pa2}\,(\text{positive-sequence component at double line-frequency})}+\underbrace{\frac{U_m^+I_m^+}{U_{\rm dc}}\cos(2\omega t+\theta^++\varphi^+)}_{i^-_{pa2}\,(\text{negative-sequence component at double line-frequency})}$$
$$+\underbrace{\frac{U_m^+I_m^-}{U_{\rm dc}}\cos(2\omega t+\theta^++\varphi^-)+\frac{U_m^-I_m^+}{U_{\rm dc}}\cos(2\omega t+\theta^-+\varphi^+)}_{i^0_{pa2}\,(\text{zero-sequence component at double line-frequency})} \tag{14d}$$

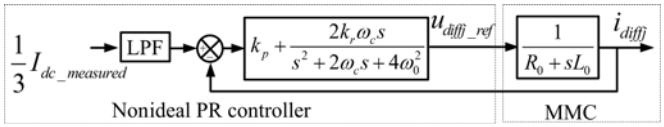

Fig. 6. Diagram of the proposed circulating current suppressing controller.

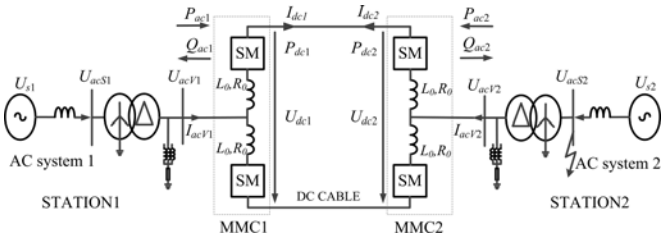

Fig. 7. Block diagram of the two-terminal MMC-HVDC transmission system.

TABLE I
PARAMETERS OF THE STUDIED SYSTEM

Items	Values
AC grid system voltage U_{s1},U_{s2}	230 kV
Short-circuit current of ac system	50 kA
Impedance angle of ac system	86°
Maximum frequency variation range of ac system	±1 Hz
Transformer ration U_s/U_v	230 kV/205.13 kV
Winding reactance of the transformer	0.15 p.u.
Dc bus rate voltage U_{dc}	400 kV
Number of SMs per arm N	250
SM capacitance C_0	6000 μF
Arm inductance L_0	90 mH
Equivalent arm resistance R_0	0.5842 Ω
DC cable resistance	0.9152 Ω
DC line reactance	20 mH
Earth reactance	3 H
Earth resistance	1 kΩ

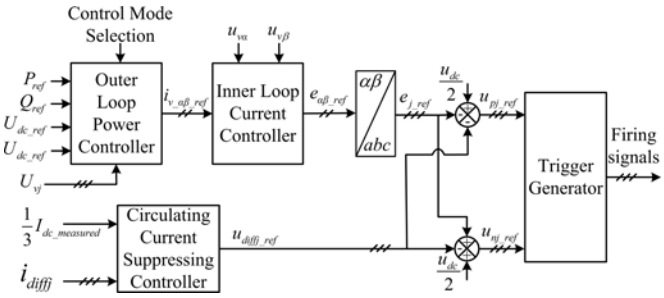

Fig. 8. Entire control structure of the MMC-HVDC transmission system.

2) making the control structure more concise, one controller for one phase;
3) resisting the ripples in dc voltage effectively.

IV. Simulation Results

A two-terminal MMC-HVDC transmission system model is established on RTDS to verify the proposed control strategy. The RTDS runs in nonreal time mode with time-step setting to 20 μs. MMC converter is simulated by the MMC5 block and the modulation method used is nearest level control [19], [25]. Fig. 7 [18], [26] shows the MMC-HVDC transmission system structure and Table I lists the main circuit parameters. The entire control structure is shown in Fig. 8. In this case scenario, station 1 controls the dc bus voltage and the reactive power, while station 2 controls the active and reactive power.

A. Evaluating the Performance of the Proposed Control Strategy Under Balanced Grid Conditions

Initially, in station 2 the circulating current suppressing controller is disabled but reenabled at $t = 0.25$ s. The active power is step changed at $t = 0.4$ s, from -300 to -400 MW. Then, at $t = 0.6$ s, the reactive power is step changed from 50 to 100 Mvar. The simulation results are shown in Fig. 9.

Fig. 9(e) and (f) shows the inner unbalanced currents and circulating currents. As can be seen, the second harmonic circulating currents are suppressed very well. In Fig. 9(c) and (d), the active power and reactive power are well regulated to their reference value with very tiny overshoot when power is step changed. The dc voltage and current are shown in Fig. 9(a) and (b). It can be seen that they are very stable during steady state.

B. Single Phase to Ground Fault Operation

Initially, station 1 operates at constant dc voltage and zero reactive power. Station 2 operates at -400 MW active power and zero reactive power. The controllers of two stations shown in Fig. 6 are disabled before $t = 0.5$ s. A single phase-to-ground fault takes place in station 2 at 0.3 s. The simulation results are shown in Figs. 10–11.

$i_{pb}, i_{nb}, i_{diffb}, i_{cirb}, i_{pc}, i_{nc}, i_{diffc}, i_{circ}$ can be deduced by the similar way

$$I_{\rm dc} = i_{pa} + i_{pb} + i_{pc} = \underbrace{\frac{3U_m^+ I_m^+}{U_{\rm dc}}\cos(\theta^+ - \varphi^+) + \frac{3U_m^- I_m^-}{U_{\rm dc}}\cos(\theta^- - \varphi^-)}_{\rm dc\ component} + \underbrace{\frac{3U_m^+ I_m^-}{U_{\rm dc}}\cos(2\omega t + \theta^+ + \varphi^-) + \frac{3U_m^- I_m^+}{U_{\rm dc}}\cos(2\omega t + \theta^- + \varphi^+)}_{\rm zero-sequence\ component\ at\ double\ line-frequency} \quad (14e)$$

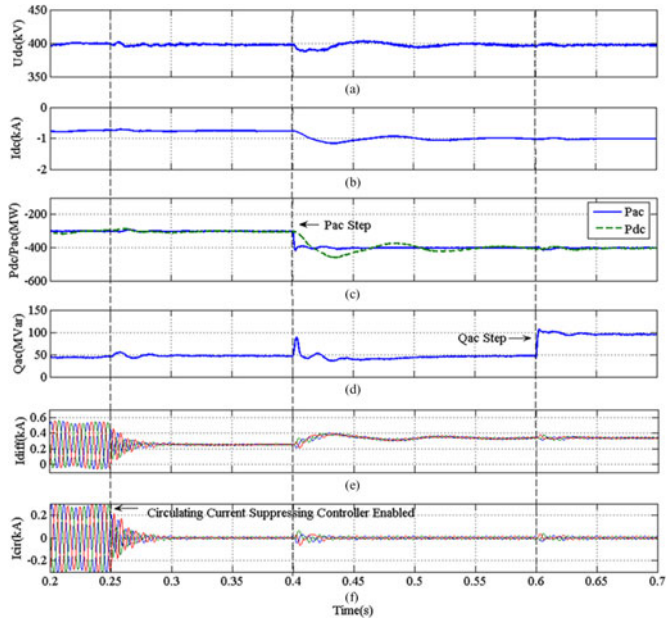

Fig. 9. Simulation results in station 2 under balanced grid conditions: (a) DC voltage. (b) DC current. (c) Active power at converter side and dc side. (d) Reactive power at converter side. (e) Inner unbalanced currents. (f) Circulating currents.

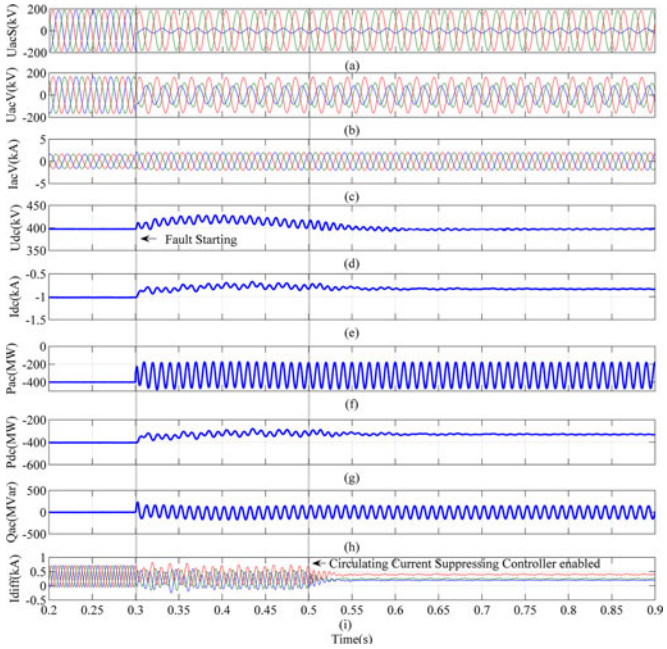

Fig. 10. Simulation results of station 2 under unbalanced grid conditions. (a) AC phase voltages at grid side, (b) AC phase voltages at converter side. (c) AC currents at converter side. (d) DC voltage. (e) DC current. (f) Active power at converter side. (g) Active power at dc-side. (h) Reactive power at converter side. (i) Inner unbalanced currents.

It is shown in Figs. 10(c) and 11(b) that the ac currents are balanced during the fault period, since the inner loop current controller suppresses the negative-sequence current significantly. However, the amplitude of ac current is increased, because the positive-sequence ac voltage is dropped. To avoid the over current phenomena of station 2, an inner loop current limiter in Fig. 3 is applied. It can be seen that the amplitude of ac current is limited to about 1.1 p.u.

The inner unbalanced currents are shown in Fig. 10(i), and their sequence components in $\alpha\beta$ reference frame are shown in Fig. 11(c)–(e). Before circulating current suppressing controller is enabled, they mainly consist of negative-sequence component at double line-frequency under balanced grid conditions, while positive-, negative-, and zero-sequence component under unbalanced grid conditions. The zero-sequence component leads to ripples in dc voltage, dc current, and dc power, which is shown in Fig. 10 (d)–(e) and (g). After the circulating current suppressing controller is enabled, the double line-frequency components in inner unbalanced currents are suppressed significantly, which is shown in Figs. 10(i) and 11(c)–(e). The ripples in dc voltage, dc current, and dc power are also suppressed, since the zero-sequence component is almost eliminated. $P_{\rm ac}$ and $Q_{\rm ac}$ are presented in Fig. 10(f) and (h). They contain fluctuations at double line-frequency during the fault period because of the negative-sequence component in ac voltage.

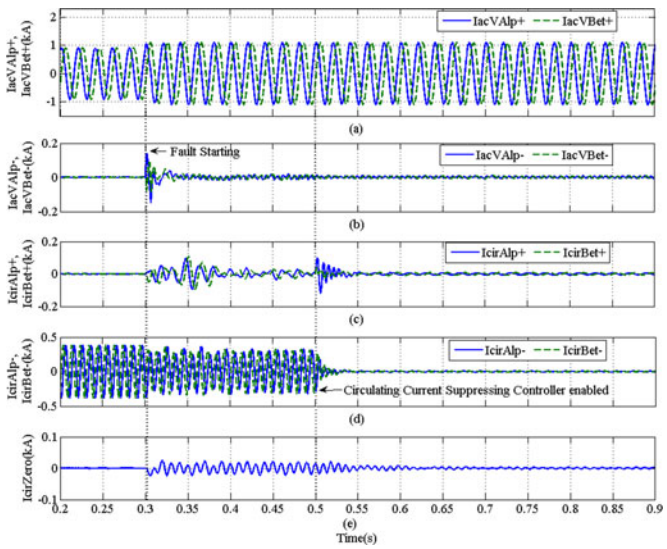

Fig. 11. Sequence components analysis for ac current and circulating current of station 2 under unbalanced grid conditions: (a) Positive-sequence component of ac current in $\alpha\beta$ frame. (b) Negative-sequence component of ac current in $\alpha\beta$ frame. (c) Positive-sequence component of circulating current in $\alpha\beta$ frame. (d) Negative-sequence component of circulating current in $\alpha\beta$ frame. (e) Zero-sequence component of circulating current.

C. Response to Frequency Variation of AC System

Fig. 12 shows the characteristics of MMC when the system frequency is step changed. Initially, station 1 operates at 400 kV dc voltage and zero reactive power, station 2 operates at -400 MW active power and zero reactive power. Circulating current suppressing controllers of two stations are enabled. The frequency of ac system in station 2 is step changed from 50 to 51 Hz at $t = 0.3$ s.

As seen from the Fig. 12, the performance of conventional method [11] begin to deteriorate when frequency steps. Conventional method [18] is also influenced with overshoot in the

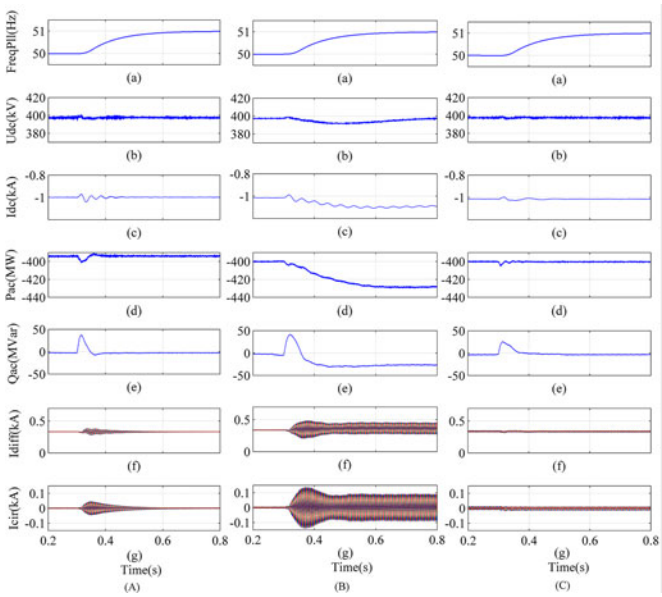

Fig. 12. Simulation results in station 2 when the frequency of ac grid is step changed: (a) Response of the PLL to frequency's step change. (b) DC voltage, (c) DC current. (d) Active power at converter-side. (e) Reactive power at converter-side. (f) Inner unbalanced currents. (g) Circulating currents. (A) Conventional method [18]. (B) Conventional method [11], (C) Proposed method.

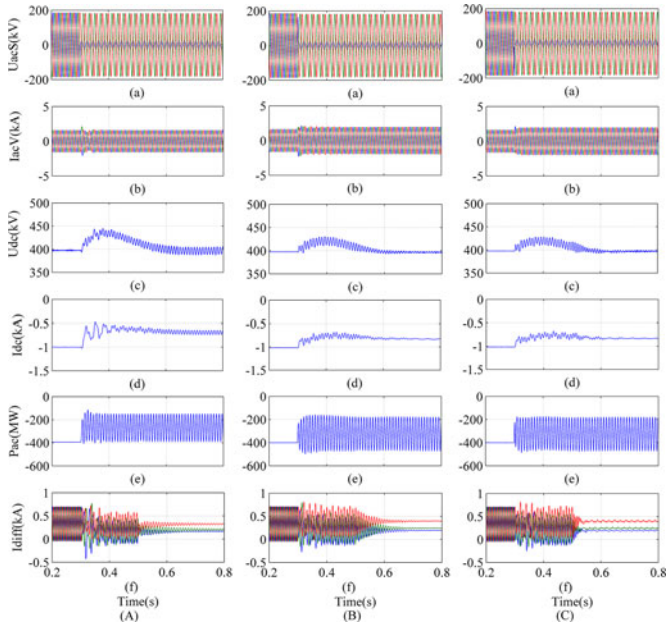

Fig. 13. MMC simulation results of station 2 under unbalanced grid conditions: (a) AC voltages at gird side. (b) AC currents at converter side. (c). DC voltage. (d) DC current. (e) Active power at converter side. (f) Inner unbalanced currents. (A) Conventional method [18]. (B) Conventional method [11] (C) Proposed method.

circulating currents. However, the proposed method has strong adaptability against frequency disturbance, which has quite small influence on the performance of circulating current suppressing controller.

D. Contrast Experiment

Fig. 13 shows the simulation results of a classic conventional circulating current suppression method in *dq* SRF [18], a typical control method in stationary frame [11], and the proposed method in stationary frame under unbalanced grid conditions. To apply unbalanced grid conditions, a single line-to-ground fault is applied at $t = 0.3$ s. The circulating current suppressing controller is disabled before $t = 0.5$ s. Since the objectives of inner loop current control are all set to suppress the negative-sequence current, all the methods show similar characteristics. Unable to suppress positive-sequence component in the circulating current is the major weakness of conventional method [18]. The dynamic performance of conventional method [11] is influenced by the high-pass filters which are used to extract the double-line frequency component from circulating current. To summarize what has been mentioned above, a comparison is made in Table II.

TABLE II
COMPARISON BETWEEN THE PROPOSED STRATEGY AND THE PREVIOUSLY INTRODUCED STRATEGIES

Items	Classic Conventional Strategy [18] in *dq* SRF	Conventional Strategy [11] in Stationary Frame	Proposed Strategy in Stationary Frame
Structure of control system	More complicated	Complicated	Concise
Performance under balanced grid conditions	Good	Good	Good
Performance under unbalanced grid conditions	Ordinary	Good	Good
Circulating current suppression ability under unbalanced grid conditions	Unable to suppress positive-sequence component	Strong	Strong
Frequency adaptive ability	Strong	Weak	Strong

V. CONCLUSION

This paper proposes a new control strategy under unbalanced grid conditions, which is based on the MMC's mathematical model and the analysis of the circulating current. It consists of inner loop current controller and circulating current suppressing controller. The inner loop current controller is designed in $\alpha\beta$ stationary frame based on nonideal PR controllers. Positive- and negative-components of the ac current can be controlled at the same time by one controller under unbalanced grid conditions. Compared to the existing dual sequence current control scheme, this approach simplifies the structure of controller and avoids the sequence components extracting from the currents.

Under unbalanced grid conditions, there are positive-, negative-, and zero-sequence components in the circulating current at double line-frequency. Circulating current suppressing controller in *abc* stationary frame is designed and it can effectively eliminate all these components. The dynamic response of the circulating current suppressing controller is fast. Nonideal PR controller is used to adapt to off-nominal system frequency conditions in the control scheme. This enables potential usage of the proposed control scheme in large-scale wind power integration.

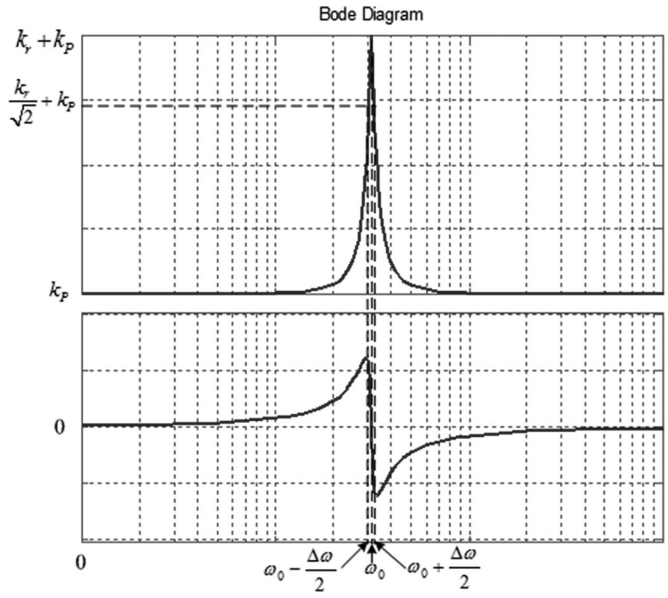

Fig. 14. Bode diagram of nonideal PR controller.

A 251-level MMC-HVDC transmission system with the proposed controllers is simulated using RTDS. The simulation results show that the controllers maintain good performance under unbalanced grid conditions.

APPENDIX

A. Detuning Parameters of the Inner Loop Current Nonideal PR Controller

The transfer function of nonideal PR controller is shown as (6b). According to (6b), a nonideal PR controller consists of proportional link and nonideal resonant link. k_r is resonant factor and k_P is proportional factor, which does not influence the bandwidth of the nonideal PR controller. The amplitude of nonideal PR controller is equal to the sum of k_P and k_r at ω_0 frequency. Fig. 14 shows the amplitude- and phase-frequency characteristics of nonideal PR controller. According to Fig. 14, the bandwidth of nonideal PR controller is equal to the difference between the two frequencies with amplitudes equaling to $k_p + {k_r}/{\sqrt{2}}$ [27]. It can be described as

$$|G(j\omega)| = k_P + {k_r}/{\sqrt{2}}. \tag{15}$$

According to (15), we can obtain the bandwidth of nonideal PR controller

$$\Delta f = \omega_c/\pi. \tag{16}$$

TABLE III
CIRCUIT PARAMETERS

Symbol	Quantity	Value
R_0	Equivalent arm resistance	0.5842 Ω
L_0	Arm inductance	90 mH
U_{ac}	Line voltage RMS	205.13 kV
S	Base capacity	450 MVA

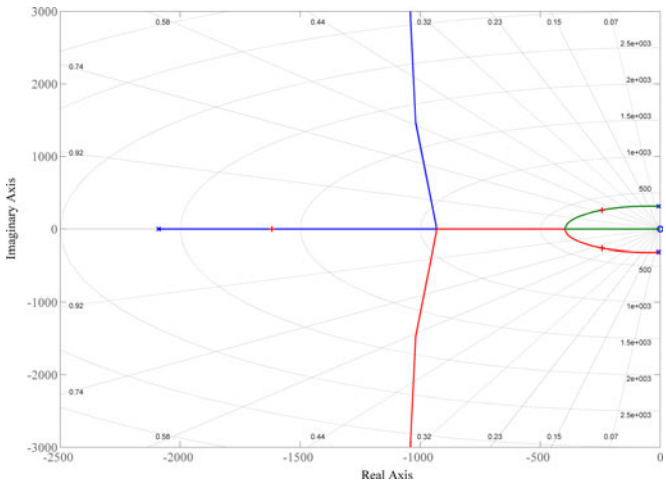

Fig. 15. Diagram of root locus.

According to (16), if the error of frequency is ±1 Hz, $\omega_c = 2\pi$ rad/s.

According to Fig. 4, the open loop transfer function is

$$G(s) = \frac{2k_p s^2 + 4\omega_c(k_p + k_r)s + 2k_p\omega_0^2}{L_0 s^3 + (R_0 + 2\omega_c L_0)s^2 + (2\omega_c R_0 + \omega_0^2 L_0)s + \omega_0^2 R_0}. \tag{17}$$

According to (17), the equation of root locus is (18), shown as the bottom of the page.

Generally, k_P should be small, in this paper, $k_P = 1$. Circuit parameters are shown in Table III, which should be transformed to p.u. The root locus is shown as Fig. 15. If the damping factor is about 0.707, $k_r = 33.2$. Three poles of the close loop system are -1578.8, $-261.8 + \text{j}248.9$, $-261.8 - \text{j}248.9$.

The close loop transfer function is (19), shown as the bottom of the page.

The Bode diagram is shown as Fig. 16. At $\omega = 314$ rad/s ($f = 50$ Hz), $L(\omega) = 1.13 \times 10^{-3}$ dB, $\varphi(\omega) = -0.282°$. At

$$G(s)^* = \frac{4\omega_c k_r s}{L_0 s^3 + (R_0 + 2\omega_c L_0 + 2k_P)s^2 + (2\omega_c R_0 + \omega_0^2 L_0 + 4\omega_c k_P)s + \omega_0^2 R_0 + 2k_P\omega_0^2} = -1 \tag{18}$$

$$\phi(s) = \frac{2k_p s^2 + 4\omega_c(k_p + k_r)s + 2k_p\omega_0^2}{L_0 s^3 + (R_0 + 2\omega_c L_0 + 2k_p)s^2 + (2\omega_c R_0 + \omega_0^2 L_0 + 4\omega_c(k_p + k_r))s + (R_0 + 2k_p)\omega_0^2} \tag{19}$$

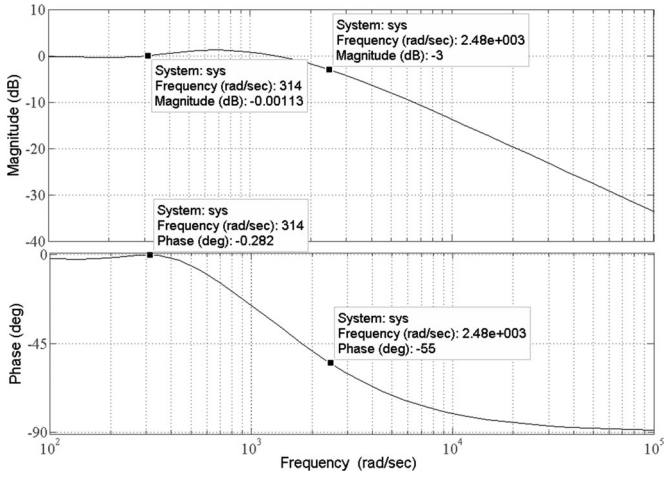

Fig. 16. Bode diagram of the close loop control system.

$\omega = 2480$ rad/s ($f = 395$ Hz), $L(\omega) = -3$ dB, $\varphi(\omega) = -55°$. The close loop control system has enough bandwidth.

B. Implementation of the Nonideal PR Controller

For implementing the nonideal PR controller, it is necessary to discretize the transfer function (6b). To avoid the creation of algebraic loops in the transformation, the bilinear transformation in [28]–[30] is employed

$$s = \frac{2}{T}\frac{z-1}{z+1}. \tag{20}$$

A discrete transfer function can be derived by substituting s in (6b) with (20)

$$G(z) = k_p + \frac{b_0 + b_1 \cdot z^{-1} + b_2 \cdot z^{-2}}{1 + a_1 \cdot z^{-1} + a_2 \cdot z^{-2}}. \tag{21}$$

where $b_0 = \frac{4k_r\omega_c T}{4+4\omega_c T+T^2\omega_0^2}$, $b_1 = 0$, $b_2 = \frac{-4k_r\omega_c T}{4+4\omega_c T+T^2\omega_0^2}$, $a_1 = \frac{-8+2T^2\omega_0^2}{4+4\omega_c T+T^2\omega_0^2}$, $a_2 = \frac{4-4\omega_c T+T^2\omega_0^2}{4+4\omega_c T+T^2\omega_0^2}$. T is the sample period of the control system.

REFERENCES

[1] R. Marquardt, "Modular multilevel converter: An universal concept for HVDC-networks and extended DC-bus-applications," in *Proc. Power Electron. Int. Conf.*, Jun. 21–24, 2010, pp. 502–507.

[2] M. Glinka and R. Marquardt, "A new ac/ac-multilevel converter family applied to a single-phase converter," in *Proc. 5th Int. Conf. Power Electron. Drive System*, Singapore, Nov. 2003, pp. 16–23.

[3] J. Dorn, H. Huang, and D. Retzmann, "A new multilevel voltage sourced converter topology for HVDC applications," in *Proc. CIGRE*, Paris, France, 2008, pp. 1–8, Paper B4-304.

[4] A. Lesnicar and R. Marquardt, "An innovative modular multilevel converter topology suitable for a wide power range," in *Proc. IEEE Bologna Power Tech Conf.*, vol. 3, 2003.

[5] H. S. Song and K. Nam, "Dual current control scheme for PWM converter under unbalanced input voltage conditions," *IEEE Trans. Ind. Electron.*, vol. 46, no. 5, pp. 953–959, Oct. 1999.

[6] M. Saeedifard and R. Iravani, "Dynamic performance of a modular multilevel back-to-back HVDC system," *IEEE Trans. Power Del.*, vol. 25, no. 4, pp. 2903–2912, Oct. 2010.

[7] P. B. Darji and A. M. Kulkarni, "Dynamic performance of a modular multi-level converter based HVDC terminal under unbalanced AC grid conditions," in *Proc. 10th Int. Conf. AC DC Power Transmiss.*, 2012, pp. 1–6.

[8] F. Liu, A. I. Maswood, Y. Kang, Y. Zhang, and S. Duan, "Proportional-resonant current control for three-phase three-level rectifier," in *Proc. Int. Conf. Power Eng.*, pp. 1018–1022, 2007.

[9] J. Hu and Y. He, "Modeling and control of grid-connected voltage-sourced converters under generalized unbalanced operation conditions," *IEEE Trans. Energy Convers*, vol. 23, no. 3, pp. 903–913, 2008.

[10] H. Pengfei, J. Daozhuo, Z. Yuebin, G. Jie, and L. Zhiyong, "Study of the proportional resonant control based modular multilevel converter," in *Proc. 3rd Int. Conf. Int. Conf. Digital Manuf. Autom.*, 2012, pp. 810–813.

[11] Z. Yuebin, J. Daozhuo, G. Jie, H. Pengfei, and L. Zhiyong, "Control of modular multilevel converter based on stationary frame under unbalanced AC system," in *Proc. 3rd Int. Conf. Digital Manuf. Autom.*, 2012, pp. 293–296.

[12] Q. Tu, Z. Xu, and L. Xu, "Reduced switching-frequency modulation and circulating current suppression for modular multilevel converters," *IEEE Trans. Power Del.*, vol. 26, no. 3, pp. 2009–2017, Jul. 2011.

[13] A. Antonopoulos, L. Angquist, and H. P. Nee, "On dynamics and voltage control of the modular multilevel converter," in *Proc. 13th Eur. Conf. Power Electron. Appl.*, 2009, pp. 1–10.

[14] Q. Tu, Z. Xu, and J. Zhang, "Circulating current suppressing controller in modular multilevel converter," in *Proc. IEEE 36th Annu. Conf. Ind. Electron. Soc.*, 2010, pp. 3198–3202.

[15] Q. R. Tu, Z. Xu, H. Huang, and J. Zhang, "Parameter design principle of the arm inductor in modular multilevel converter based HVDC," in *Proc. Int. Conf. Power Syst. Technol.*, 2010, pp. 1–6.

[16] J. W. Moon, C. S. Kim, J. W. Park, D. W. Kang, and J. M. Kim, "Circulating current control in MMC under the unbalanced voltage," *IEEE Trans. Power Del.*, vol. 28, no. 3, pp. 1952–1959, Jul. 2013.

[17] J. Qin and M. Saeedifard, "Predictive control of a modular multilevel converter for a back-to-back HVDC system," *IEEE Trans. Power Del.*, vol. 27, no. 3, pp. 1538–1547, Jul. 2012.

[18] Q. Tu, Z. Xu, Y. Chang, and L. Guan, "Suppressing DC voltage ripples of MMC-HVDC under unbalanced grid conditions," *IEEE Trans. Power Del.*, vol. 27, no. 3, pp. 1332–1338, Jul. 2012.

[19] S. Kouro, R. Bernal, H. Miranda, C. A. Silva, and J. Rodriguez, "High-performance torque and flux control for multilevel inverter fed induction motors," *IEEE Trans. Power Electron.*, vol. 22, no. 6, pp. 2116–2123, Nov. 2007.

[20] M. Glinka and R. Marquardt, "A new AC/AC multilevel converter family," *IEEE Trans. Ind. Electron.*, vol. 52, no. 3, pp. 662–669, Jun. 2005.

[21] S. Rohner, S. Bernet, M. Hiller, and R. Sommer, "Modulation, losses, and semiconductor requirements of modular multilevel converters," *IEEE Trans. Ind. Electron.*, vol. 57, no. 8, pp. 2633–2642, Aug. 2010.

[22] H. Nazifi and A. Radan, "Current control assisted and non-ideal proportional-resonant voltage controller for four-leg three-phase inverters with time-variant loads," in *Proc. Power Electron., Drive Syst. Technol. Conf.*, Feb. 13–14, 2013, pp. 355–360.

[23] A. Yazdani and R. Iravani, "A unified dynamic model and control for the voltage sourced converter under unbalanced grid conditions," *IEEE Trans. Power Del.*, vol. 21, no. 3, pp. 1620–1629, Jul. 2006.

[24] M. Guan and Z. Xu, "Modeling and control of a modular multilevel converter-based HVDC system under unbalanced grid conditions," *IEEE Trans. Power Electron*, vol. 27, no. 12, pp. 4858–4867, Dec. 2012.

[25] Q. Tu and Z. Xu, "Impact of sampling frequency on harmonic distortion for modular multilevel converter," *IEEE Trans. Power Del.*, vol. 26, no. 1, pp. 298–306, Jan. 2011.

[26] State Power Economic Research Institute, "Technical exchange about Dalian and Zhoushan flexible dc transmission projects," unpublished, pp. 23–24.

[27] Z. Qing-Lin, G. Xiao-Qiang, and W. Wei-Yang, "Research on control strategy for single-phase grid-connected inverter," *Proc.Chin. Soc. Electr. Eng.*, vol. 27, no. 16, pp. 60–64, 2007.

[28] H. Krishna, "Computational aspects of the bilinear transformation based algorithm for S-plane to Z-plane mapping," *IEEE Trans. Automat. Control*, vol. 33, no. 11, pp. 1086–1087, Nov. 1988.

[29] A. G. Yepes, F. D. Freijedo, J. Doval-Gandoy, O. Lopez, J. Malvar, and P. Fernandez-Comesana, "Effects of discretization methods on the performance of resonant controllers," *IEEE Trans. Power Electron.*, vol. 25, no. 7, pp. 1692–1712, Jul. 2010.

[30] S. A. Khajehoddin, M. K. Ghartemani, P. Jain, and A. Bakhshai, "A frequency adaptive resonant controller for fixed point digital implementation at high sampling frequency," in *Proc. IEEE Eenrgy Convers. Congr. E*, pp. 2557–2561, 2011.

Shaohua Li was born in Hunan, China, in 1982. He received the B.S. degree in electrical engineering from Hunan University, Changsha, China, in 2005, and the M.S. degree in control engineering from Xi'an Jiaotong University, Xi'an, China, in 2008. He is currently working toward the Ph.D. degree in electrical engineering at Xi'an Jiaotong University.

He has been an Engineer at XJ Electric Co., Ltd., Henan, China, since 2008. His research interest includes HVDC and voltage-source converter HVDC system.

Xiuli Wang (M'99) was born in June, 1961. She received the M.S and Ph.D. degrees in electrical engineering from Xi'an Jiaotong University, Xi'an, China, in 1985 and 1997, respectively.

She has been a Professor in the Electrical Engineering Department, Xi'an Jiaotong University since 2001. Her research interests include power system planning, power market, power system reliability, and HVDC transmission.

Zhiqing Yao was born in Jiangsu, China, in 1960. He received the B.E. degree from Jiangsu University, Zhengjiang, China. He is currently working toward the Ph.D. degree in electrical engineering at the Huazhong University of Science and Technology, Wuhan, China.

He is currently with Xuchang KETOP Electrical Research Institute, Henan, China. His research interests include power system protection and control, HVDC, FACTS, power converters, and application of power electronics in renewable power system.

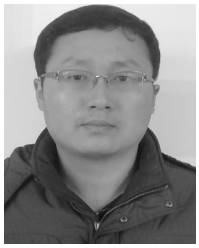

Tai Li was born in Henan, China, in 1980. He received the B.S. degree in electrical engineering from the Zhengzhou University of Light Industry, Zhengzhou, China, in 2004, and the M.S. degree in electrical engineering from Southwest Jiaotong University, Chengdu, China, in 2008.

He has been an Engineer at XJ Electric Co., Ltd., Henan, China, since 2008. His main interests include the control and protection system of HVDC and MMC-HVDC.

Zhong Peng was born in Hunan, China, in 1986. He received the B.S. degree in electrical engineering from Hunan Institute of Engineering, Xiangtan, China, in 2009, and the M.S. degree in electrical engineering from Hunan University, Changsha, China, in 2011.

He has been an Engineer at XJ Electric Co., Ltd., Henan, China, since 2011. His main research interests include the control and protection system of HVDC and MMC-HVDC.